Bioconjugate Chemistry

Article

pubs.acs.org/bc

Parallel Multifunctionalization of Nanoparticles: A One-Step Modular Approach for in Vivo Imaging

Hugo Groult,[†] Jesús Ruiz-Cabello,[†,‡] Juan Pellico,[†,‡] Ana V. Lechuga-Vieco,[†] Riju Bhavesh,[†] Moreno Zamai,[§] Elena Almarza,[∥] Inés Martín-Padura,[⊥] Eugenio Cantelar,[#] María P. Martínez-Alcázar,[¶] and Fernando Herranz*[,†]

[†]Advanced Imaging Unit, Department of Atherotrombosis, Imaging and Epidemiology, Fundación Centro Nacional de Investigaciones Cardiovasculares (CNIC) and CIBER de Enfermedades Respiratorias (CIBERES), Melchor Fernández Almagro, 3, 28029 Madrid, Spain

[‡]Universidad Complutense de Madrid (UCM), Plaza Ramón y Cajal s/n Ciudad Universitaria, 28040 Madrid, Spain

[§]Microscopy Unit and [⊥]Department of Vascular Biology and Inflammation, Fundación Centro Nacional de Investigaciones Cardiovasculares (CNIC)Melchor Fernández Almagro, 3, 28029 Madrid, Spain

[∥]Division of Haematopoietic Innovative Therapies. Centro de Investigaciones Energéticas, Medioambientales y Tecnológicas (CIEMAT), CIBER de Enfermedades Raras (CIBER-ER) and Instituto de Investigación Sanitaria Fundación Jiménez Díaz. (IIS-FJD, UAM), 28040Madrid, Spain

[#]Departamento de Física de Materiales, Facultad de Ciencia de la Universidad Autónoma de Madrid. Ciudad Universitaria de Cantoblanco, 28049 Madrid, Spain

[¶]Chemistry Department, Analytical Chemistry Section, Facultad de Farmacia, Universidad CEU-San Pablo, Urbanizacion Monteprincipe, Boadilla del Monte, 28660 Madrid, Spain

S *Supporting Information*

ABSTRACT: Multifunctional nanoparticles are usually produced by sequential synthesis, with long multistep protocols. Our study reports a generic modular strategy for the parallel one-step multifunctionalization of different hydrophobic nanoparticles. The method was designed and developed by taking advantage of the natural noncovalent interactions between the fatty acid binding sites of the bovine serum albumin (BSA) and the aliphatic surfactants on different inorganic nanomaterials. As a general example of the approach, three different nanoparticles—iron oxide, upconverting nanophosphors, and gold nanospheres—were nanoemulsified in water with BSA. To support specific applications, multifunctional capability was incorporated with a variety of previously modified BSA modules. These modules include different conjugated groups, such as chelating agents for ^{68}Ga or ^{89}Zr and ligand molecules for enhanced in vivo targeting. A large library of 13 multimodal contrast agents was developed with this convergent strategy. This platform allows a highly versatile and easy tailoring option for efficient incorporation of functional groups. Finally, as demonstration of this versatility, a bimodal (PET/MRI) probe including a maleimide-conjugated BSA was selectively synthesized with an RGD peptide for in vivo imaging detection of tumor angiogenesis.

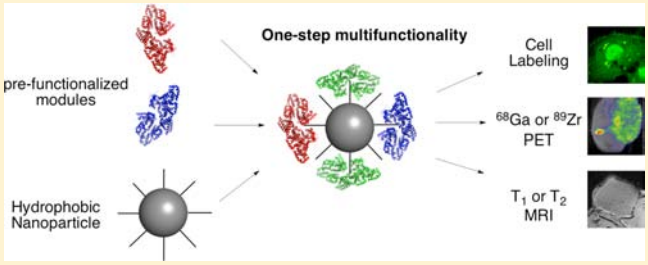

INTRODUCTION

Because of their unique physicochemical properties at the molecular and cellular levels, inorganic nanoparticles are particularly interesting for in vivo medical imaging and drug delivery.[1,2] Thermal decomposition is one of the most used synthetic methods rendering crystalline and highly monodispersed hydrophobic NPs. These particles are stabilized with surfactants made of long aliphatic chain like oleic acid or oleylamine, and are therefore dispersible only in different organic solvents.[3,4] Consequently, the multiple steps for the final multifunctionalization start with the hydrophilic conversion of the NPs to obtain a probe stable in physiological media, by ligand exchange,[5] direct chemical modification of the surfactant,[6,7] or stabilization within a hydrophilic coating matrix.[8,9] The various hydrophilic coating matrix approaches proposed include inorganic or organic encapsulation, such as polymeric or protein-based, and micellar or liposomal structures.[10−12] This hydrophilic coating provides improved colloidal stability to the NPs, protection from opsonization, and biocompatibility.[13] It is also of paramount importance that the

Received: November 21, 2014
Revised: December 9, 2014
Published: December 11, 2014

coating allows stable drug entrapment or further functionalization like attachment of targeting ligand and additional imaging probes.[10,14] BSA fulfills all of these requirements, as several research groups have demonstrated.[15] Albumin is the most abundant protein in the blood and has crucial biological functions, including the transport of hydrophobic molecules to the tissues.[16] BSA as an organic nanoparticle or coating for inorganic NPs has also been reported to improve the in vivo properties of the probe.[15,17−19] Schäffler et al. and others recently showed that albumin−NP conjugates not only have improved biocompatibility but also may be used as a potential tool for organ targeting like brain or lungs.[20,21] Nonetheless, albumin conjugation on NPs is always made on an existing hydrophilic coating, bringing into play covalent or ionic binding or just simple adsorption.[22−24] As far as we know, no method that directly transfers hydrophobic OA/OM coated NPs in aqueous phase with BSA has previously been described.

Multifunctionality is a unique characteristic of nanomaterials; the possibility of introducing several imaging agents, plus biological targeting moieties and drugs, is one of the most prominent features of this new type of chemistry. However, this multiplex incorporation presents some inherent problems, particularly the need for various complex sequential steps, in turn reducing the overall yield and lowering the reproducibility.[25−27] This is especially relevant nowadays for creating new PET/MRI and Fluorescence/MRI agents with the idea of combining sensitivity and improved spatial resolution.[23,25,28]

Following a modular approach, our proposal is different: by the hydrophobic interactions between fatty acid binding sites of albumin and the aliphatic chains on the coating of the NPs we demonstrate how the parallel multifunctionalization is achievable for a large variety of nanoparticles and coating possibilities. As for nanoparticles we apply our approach to iron oxide nanoparticles, up-converting nanophosphors, and gold nanoparticles. By using each type of NP with different combinations of natural BSA and fractions of premodified BSA with Alexa Fluor647, DOTA (chelator for ^{68}Ga), DFO (chelator for ^{89}Zr), or maleimide reactive moiety, a large library of multifunctional contrast agents (BSA-NPs) was prepared. After a thorough characterization of all the BSA-NPs the capacity of the platform for targeted bioimaging was finally assessed. For this, a bimodal contrast agent from the library was selected for RGD conjugation and its accumulation in a mouse model of cancer was studied by PET and MRI.

RESULTS AND DISCUSSION

Synthesis and Physicochemical Characterization of BSA Coated IONP, UCNP, and AuNP. OA-IONP (**1**), OA-UCNP (**2**), and OM-AuNP (**3**) were first prepared by decomposition of organometallic precursors at high temperature with small variations according to each type of metal core (detailed protocols are shown in the experimental section). UCNP refers to a family of nanoparticles comprising a wide range of different types of inorganic core.[6] In this study, we have used a core composed of a $NaGdF_4$ host matrix with ytterbium (Yb) and thulium (Tm) lanthanide dopants embedded in a $NaGdF_4$ passive shell, abbreviated $NaGdF_4$:Yb,Tm@$NaGdF_4$. In all cases, the synthesis yielded hydrophobic NPs with narrow size distribution (polydispersity index, pdi <0.25 nm) and small hydrodynamic size between 10 and 30 nm depending on the type of NP (Supporting Information Table S1).

TEM images for the hydrophobic nanoparticles are shown in Figure 1. The first step was to demonstrate the feasibility of

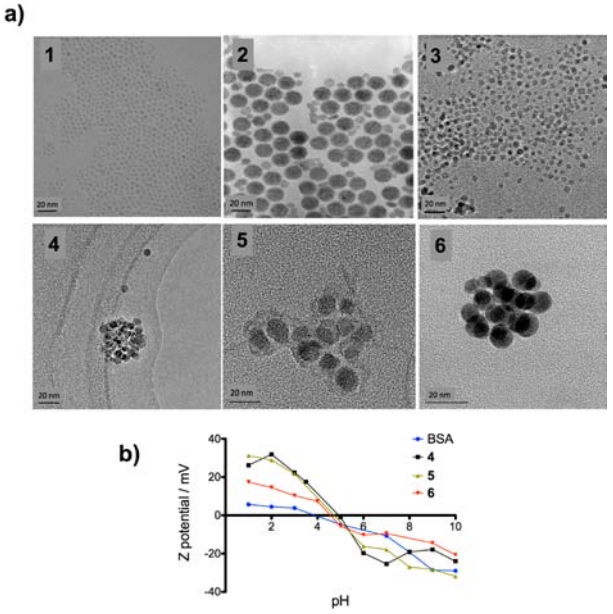

Figure 1. (a) TEM images of hydrophobic NPs (**1**), (**2**), (**3**), and BSA coated NPs (**4**), (**5**), (**6**). (b) Zeta potential of BSA coated NPs (**4**), (**5**), (**6**) as a function of pH.

aqueous stabilization through BSA binding to the aliphatic chains. This was achieved, as represented in Scheme 1a, by adapting a simple, fast, and reproducible nanoemulsion method.[29]

The nanoemulsion involved mixing a small volume of NPs dispersed in hexane with an aqueous phase (phosphate buffer, pH 7.2), 1/10 in v/v, containing BSA protein. Upon homogenization and stirring, an oil-in-water nanoemulsion is formed and gradual evaporation of the organic phase leads to a stable colloidal aqueous solution of BSA-IONP (**4**), BSA-UCNP (**5**), and BSA-AuNP (**6**). Stabilization was achieved by hydrophobic van der Waals interactions between the surfactant (OA or OM) of the hydrophobic NPs and the fatty acid binding sites of the albumin. The BSA-stabilized NPs did not show redispersion, if mixed again with hexane phase (1/1 in volume). This method is more flexible, easier, and faster than the widely common adsorption, conjugation, or desolvation routes used to coat NPs with albumin.[20,23,24] To confirm that the stabilization was achieved via hydrophobic interactions between OA and BSA fatty acid binding sites, several control reactions were performed. These consisted of repeating the nanoemulsion formulation with a pretargeted BSA, in which the fatty acid binding sites were previously saturated with free OA. As expected, the BSA was not able to bind to the surface, making the formation of a stable aqueous colloidal solution of nanoparticles **4**, **5**, and **6** impossible. This confirms that the binding origin is mainly through hydrophobic interactions and not simple adsorption on the surface of the NPs. This straightforward use of the fatty acid binding sites of BSA simplifies the process against other synthetic strategies that use multiple steps and/or harsh reaction conditions. Final hydrodynamic sizes of **4**, **5**, and **6** were 97.2, 94.3, and 102.5 nm with pdi below 0.25, showing that this approach leads to very homogeneous dispersions with high reproducibility (Table 1).

dx.doi.org/10.1021/bc500536y | Bioconjugate Chem. 2015, 26, 153−160

Scheme 1. (a) Modules for Combination in the Nanoemulsion Process; (b) Nanoemulsion Step with Selected Modules (Many Other Combinations Are Possible); (c) Library of Multifunctional Nanoparticles Synthesized in This Work

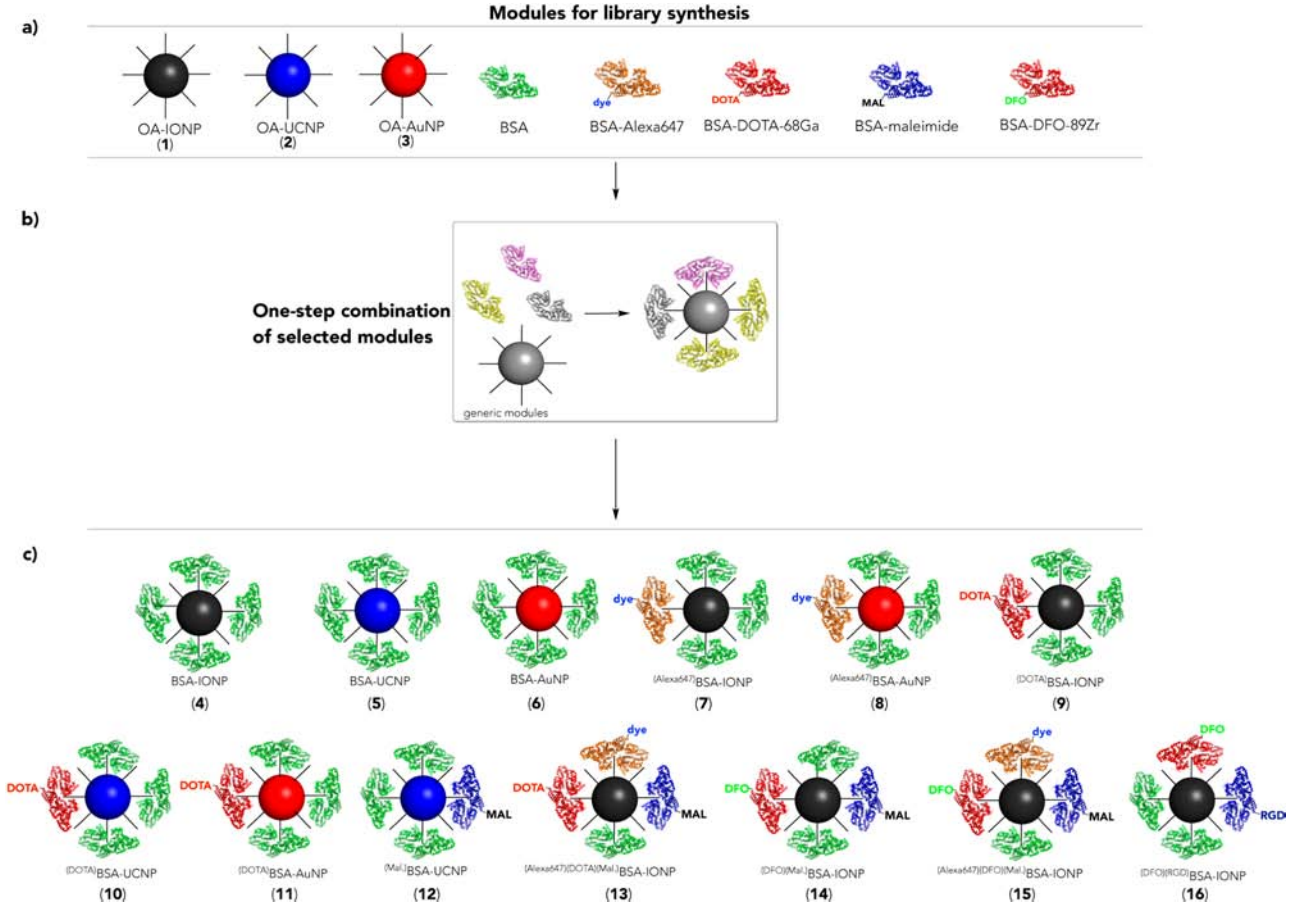

Table 1. Library of the BSA-NPs Contrast Agents: Main Physicochemical Properties and Imaging Modalities

BSA-NPs	nanoparticle #	% modified BSA	size (nm)	pdi	zeta potential (mV)	imaging properties
BSA-IONP	4	n.a.	97.2	0.18	−19.7	T_2 MRI
BSA-UCNP	5	n.a	94.3	0.19	−17.9	T_1 MRI/Fluorescence
BSA-AuNP	6	n.a.	102.5	0.15	−9.5	UV−vis/fluorescence
$^{(Alexa647)}$BSA-IONP	7	3% Alexa647	93.0	0.15	−13.5	T_2 MRI/Fluorescence
$^{(Alexa647)}$BSA-AuNP	8	3% Alexa647	108.9	0.22	−11.1	UV−vis/fluorescence/FRET
$^{(DOTA)}$BSA-IONP	9	8% DOTA	104.9	0.17	−10.8	T_2 MRI/PET
$^{(DOTA)}$BSA-UCNP	10	8% DOTA	78.7	0.20	−25.7	T_1 MRI/Fluorescence/PET
$^{(DOTA)}$BSA-AuNP	11	8% DOTA	87.5	0.13	−19.8	PET/UV−vis
$^{(Mal.)}$BSA-UCNP	12	30% Mal	100.9	0.15	−23.1	T_1 MRI/Fluorescence/targeting
$^{(Alexa647)(DOTA)(Mal.)}$BSA-IONP	13	6% Alexa647 3% DOTA 30% Mal	90.2	0.19	−8.9	T_2 MRI/PET/Fluorescence/ targeting
$^{(DFO)(Mal.)}$BSA-IONP	14	20% DFO 20% Mal	91.9	0.18	−13.9	T_2 MRI/PET/targeting
$^{(Alexa647)(DFO)(Mal.)}$BSA-IONP	15	6% Alexa647 20% DFO 15% Mal	78.4	0.16	−12.0	T_2 MRI/PET/Fluorescence/ targeting
$^{(DFO)(RGD)}$BSA-IONP	16	20% DFO 20% RGD	94.2	0.15	−14.5	T_2 MRI/PET/Angiogenesis

TEM images shown in Figure 1a confirm that the sizes match with the formation of well-defined small clusters made up of a few hydrophobic self-assembled NPs and surrounded by the BSA. Colloidal stability was checked by measuring the zeta-potential (ζ) variation, as a function of the pH (Figure 1b). As expected, it followed the same evolution as the electric charge of the BSA protein, with no net superficial charge around the BSA isoelectric point (pH 4.7, 25 °C) and a negative potential at physiological pH, preventing aggregation by strong repulsive electrostatic interactions and steric effects. The presence of protein on the nanoparticle surface was further characterized by infrared spectroscopy (FTIR, Supporting Information Figure S1), thermogravimetric analysis (Supporting Information Figure S2), and mass spectroscopy (MS, Supporting Information Figure S3). The FTIR of the three types of BSA-stabilized particles ((**4**), (**5**), and (**6**)), show the characteristic absorption spectrum of the protein, with bands at 3284, 1642, 1530, and 1391 cm^{-1} together with signals of the NP

dx.doi.org/10.1021/bc500536y | *Bioconjugate Chem.* 2015, 26, 153−160

hydrophobic surfactant: OA/OM aliphatic chain moiety at 2920 cm^{-1} (νa C−H), 2850 cm^{-1} (νs C−H), 1641 cm^{-1} (νs C═O) 1576 cm^{-1}, 1436 cm^{-1} (ν C−N), and 1534 cm^{-1} (ν N−H) and inorganic core (for example Fe−O at 580 cm^{-1} for IONP). Thermogravimetric analysis (TGA) shows that organic coating (corresponding to the removal of protein and surfactant between 300 and 900 °C) represents approximately 43% (**4**), 50% (**5**), and 27% (**6**) of the total weight of each NP. The smaller amount of organic phase for gold nanoparticles is most likely due to a lower amount of OM on the surface of **3** in comparison to the use of OA. Mass spectrometry data of the three kinds of NPs (analyzed in positive ionization) were representative of the expected BSA adducts and was similar to the unbound BSA control spectrum.

Library of Multifunctional Nanoparticles by Modular Integration of Prelabeled BSA. Through traditional bioconjugation (especially succinimide-activated carboxylic groups) it is possible to incorporate a covalent linkage of additional probes and add new functionalities to the protein. One key aspect of our approach is the possibility of using the nanoemulsion method with small fractions of modified BSA in addition to the native BSA, a straightforward method of obtaining water stable and multimodal NPs. In this flexible modular approach, we have used BSA modules conjugated with (i) Alexa Fluor647 fluorophore (optical modality); (ii) DOTA chelating agent for short half-life isotope like ^{68}Ga (PET modality); (iii) DFO as chelating agent for long half-life isotope like ^{89}Zr (PET modality); and (iii) a maleimide moiety (functional group for easy attachment of a targeting peptide by click chemistry). Different combinations between hydrophobic NPs and the modified BSA modules were performed so as to obtain a large molecular imaging portfolio of multifunctional contrast agents (13 different BSA-NPs, Scheme 1).

Table 1 summarizes the different composition, physicochemical properties, and imaging possibilities of each contrast agent. Hydrodynamic sizes of the BSA-NPs ranged between 78.4 and 108.9 nm with a pdi for all of them below 0.25 and a negative zeta potential ζ at neutral pH. It demonstrates the versatility of this modular approach, in all cases resulting in very homogeneous and particularly reproducible dispersions.

Imaging Modalities Provided by the Inorganic Core of the Nanoparticles. Our modular approach is valid for different types of nanoparticles, independently of the nature and physicochemical properties of each IONP, UCNP, and AuNP. The imaging functions of each preparation depend on the core of the nanoparticles and the modified BSA modules in the coating. Thus, we first evaluated the characteristics of the core of the nanoparticles **4**, **5**, and **6** as contrast agents for different imaging techniques.

Iron Oxide NP Core. Fe_3O_4 core confers superparamagnetic behavior and normally high transversal relaxivity (r_2) for T_2-weighted MRI.[3] BSA-IONP (**4**) shows a large saturation magnetization value of 70 emu g^{-1} similar to the hydrophobic particles, measured in a vibrating sample magnetometer, both displayed in Supporting Information Figure S2. This large value explains the high transversal r_2 value of 203.4 s^{-1} mM^{-1} (r_1 = 3.2 s^{-1} mM^{-1}), which confirms these particles as an excellent probe for T_2-weighted MRI (Figure 2a). This was finally evaluated by in vitro MRI with a series of dilutions in a T_2-weighted sequence (upper row of Figure 2b).

Upconverting NP Core. Upconverting nanophosphor cores display upconversion fluorescence upon 980 nm c.w. laser excitation. In our case the $NaGdF_4$:Yb,Tm@$NaGdF_4$ allows a

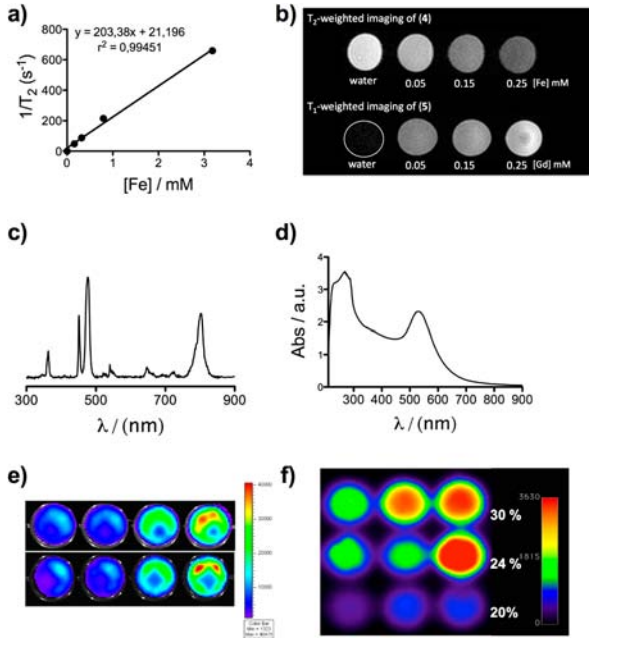

Figure 2. (a) Plot of the T_2 relaxation rate against iron concentration for BSA-IONP (**4**); (b) T_2-weighted MRI phantoms for **4** and T_1-weighted MRI phantoms for BSA-UCNP (**5**); (c) fluorescence emission spectrum for **5** after excitation with c.w. laser at 980 nm; (d) absorbance spectrum for BSA-AuNP, (**6**). (e) In vitro fluorescence imaging of nanoparticles $^{(Alexa647)}$BSA-IONP (**7**) and $^{(Alexa647)}$BSA-AuNP (**8**) and (f) in vitro PET imaging of nanoparticles $^{(DOTA)}$BSA-UCNP (**10**, 0.5 mM, upper row), $^{(DOTA)}$BSA-IONP (**9**, 0.5 mM, middle row), and $^{(DOTA)}$BSA-AuNP (**11**, 0.25 mM, bottom row); percentages indicate radiolabeling efficiency.

strong upconversion at three distinct and simultaneous sharp emissions in UV (360 nm), visible blue (451 and 476 nm), and NIR (800 nm) as shown in Figure 2c. As proof of concept of the cell labeling capabilities of the BSA-UCNP, nanoparticles **5** were cultured for 24 h with HT1080 cells (expressing RFP). Then, the fluorescence of the internalized particles was studied using two-photon imaging (Supporting Information Figure S4). Images clearly show the signal from the nanoparticles, mainly surrounding their nucleus, when excited at 980 nm. Although the UCNP are mainly designed for optical imaging, here the presence of gadolinium in the core also confers paramagnetic properties and thus MRI contrast agent capability. The longitudinal (r_1) and transversal (r_2) relaxivity values of **5** were measured (r_1 = 0.8 s^{-1} mM^{-1} and r_2 = 2.5 s^{-1} mM^{-1}). The relaxometric properties are modest since a compromise must be reached between relaxometric and optical properties: the better the fluorescence, the lower the r_1 value (due to size effects). These values show that UCNP based contrast agents can also be tuned for T_1-weighted MRI applications, as the results summarized in the bottom row of Figure 2b demonstrate. A positive contrast is observed upon increase in the nanoparticle concentration in comparison with water (encircled dark signal).

Gold NP Core. The most prominent feature of gold nanoparticles is their surface plasmon resonance due to the electromagnetic confinement, giving rise to their characteristic color variations with size. This has been extensively exploited, particularly for in vitro applications.[30] The UV−vis absorbance spectrum of the BSA-AuNP (**6**) presented in Figure 2d confirms this, as proof of concept of the suitability of the BSA-AuNP series for these applications. The spectrum shows the

dx.doi.org/10.1021/bc500536y | Bioconjugate Chem. 2015, 26, 153−160

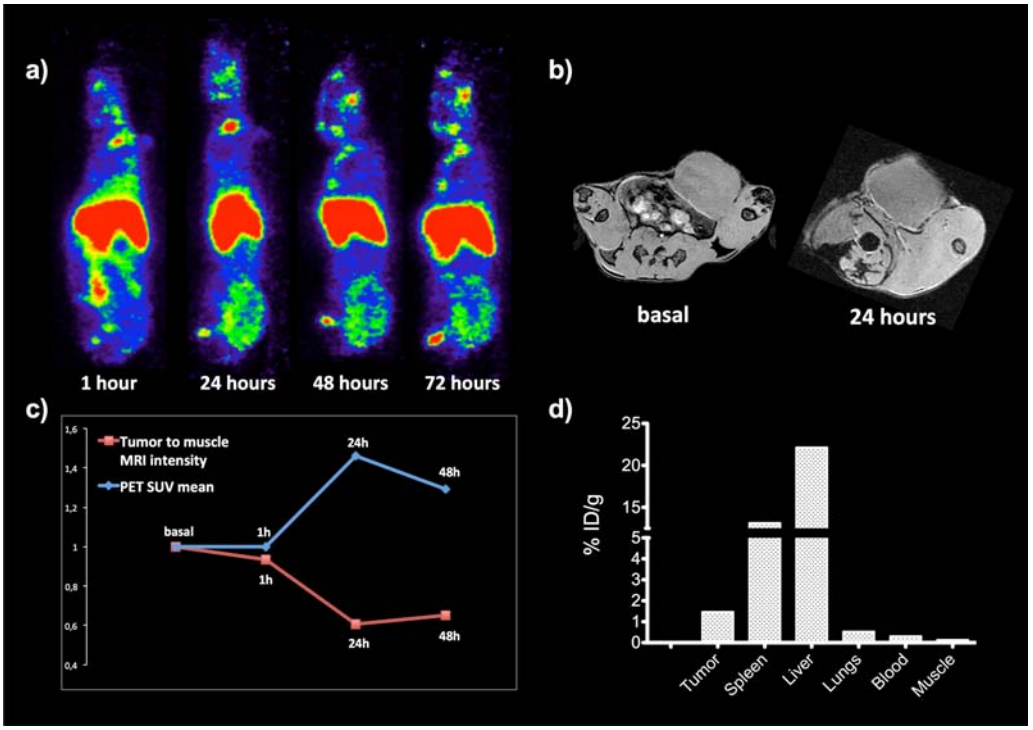

Figure 3. (a) PET imaging of $^{(89Zr)(RGD)}$BSA-IONP (**16**) at different time points postinjection in mouse bearing allograft tumor. (b) Axial T_2 weighted MRI located at the tumor before and 24 h postinjection. (c) Standardized uptake value (SUV) of tumor (blue) and relative MRI mean intensities at different days postinjection (to the intensity in a ROI located in the leg muscles, in red). (d) Activity measured in a gamma counter of specific organs (72 h postinjection).

typical broad absorbance band for albumin around 250 nm and the one typical for gold nanoparticles of this size at about 590 nm.[30]

Characterization of the Functionalities Provided by the BSA Modules of the Contrast Agents. The fluorescence and PET imaging properties provided by the different modified BSA modules were characterized (Figure 2).

*Alexa Fluor 647 Conjugated BSA (**7**, **8**, **13**, and **15**).* The $^{(Alexa647)}$BSA module was added at maximum 6% weight of the total BSA weight used. The presence of the dye, in nanoparticles **7** and **8**, was checked by fluorescence molecular tomography using several phantoms of varying concentration for nanoparticles (Figure 2e).

*DOTA Conjugated BSA (**9**, **10**, **11**, and **13**) and DFO Conjugated BSA (**14**, **15**, and **16**).* . To obtain nanoparticles ready for PET imaging, radiometals and chelators are commonly incorporated in the coating.[31] We have demonstrated the benefit of our proposal using a short half-life isotope obtained from a generator (^{68}Ga, $t_{1/2}$ = 68 min) and a long half-life isotope delivered from a cyclotron (^{89}Zr, $t_{1/2}$ = 78.4 h). In the case of ^{68}Ga, DOTA is the most often used chelator.[32] NHS-activated DOTA was covalently attached to BSA to obtain the $^{(DOTA)}$BSA module, fractions of which were added at different proportions into the nanoemulsion formulation for synthesis of **9**, **10**, and **11** (Table 1). These particles were then labeled with $^{68}GaCl_3$ eluted from a ^{68}Ge/^{68}Ga generator. In all cases, radiolabeling yield was up to 20% (Figure 2f), calculated after subtraction of the nonspecific ^{68}Ga chelation by the native BSA coating.

In vitro PET imaging of phantoms for nanoparticles **9**, **10**, and **11** were carried out showing a strong signal over the range of concentrations (Figure 2f). The intensity for nanoparticles **11** is clearly lower due to two factors: a smaller amount of $^{(DOTA)}$BSA module on the surface and also a smaller AuNP concentration (0.25 mM of Au for **11** in comparison to 0.5 mM of Fe for **9** and Gd for **10**). In the case of ^{89}Zr, a common chelating agent is DFO.[33] A previously prepared module of BSA covalently attached to DFO groups was incorporated in **14** and **15** coating and radiolabeling yield of the probe obtained was up to 14%. All these radiolabeling yields are particularly high if we consider that the amount of $^{(chelators)}$BSA is no higher than 8% in the case of ^{68}Ga and 20% for ^{89}Zr and, from that percentage, only a fraction of chelators would be available for coordination with the radioisotope.

*Maleimide Conjugated BSA and Biofunctionalization (**12**, **13**, **14**, and **15**).* Maleimide is often used to attach biomolecules in a specific manner, through click chemistry with thiol groups.[5,34] In the synthesis of **12**, **13**, **14**, and **15** a fraction of commercial $^{(maleimide)}$BSA modules (10−20 maleimide per BSA) were incorporated. The presence of BSA bearing maleimide module in the coating of these NPs was verified by FTIR with a characteristic band from the maleimide at 1130 cm^{-1}; the example for **12** is shown in Supporting Information Figure S1. This module adds to the platform the possibility of an easy functionalization with thiol bearing targeting molecule. This was further verified by the conjugation of a thiol derived cyclic RGD peptide on the coating of **14**.

Evaluation of Cytotoxic Effects and Biodistribution. Cytotoxicity studies were carried out for each type of inorganic core with a full natural BSA coating (**4**, **5**, and **6**). Cytotoxicity was evaluated after incubation of each agent at different doses with C57BL/6 mouse adult fibroblasts (MAFs) over 72 h. As displayed in Supporting Information Figure S5, in the cell viability assay we did not observe any toxic effect for **4** and **6**, only for **5**, when a slightly more pronounced effect is observed at the higher dose. An additional experiment studied the

dx.doi.org/10.1021/bc500536y | *Bioconjugate Chem.* 2015, 26, 153−160

internalization of **7** in the MEFs at 40 $\mu g \cdot mL^{-1}$ over 24 h by fluorescent cytometry analysis. The presence of AlexaFluor 647 conjugated BSA fraction in the coating of **7** enhanced the sensitivity for detection and thus the possibility of observing the cellular internalization of the nanoparticle by flow cytometry (Supporting Information Figure S5). Cell fluorescence and SSC (side-scattered light-related to cell internal complexity) increased in the cells treated and confirmed a high uptake of the NPs (Supporting Information Figure S5).[35] The strain caused on MAFs by such high internalization can explain the small cytotoxic effect observed at the highest doses. Gold and gadolinium inorganic cores have been described as less biocompatible than iron oxide,[36,37] also explaining the higher apoptotic occurrence found for **5**. As expected, the elimination of the hydrophobic character on the surface, due to the BSA coating, translates to a very low toxicity.[38]

The biodistribution of BSA nanoparticles was studied by fluorescence, using also nanoparticle **7** in mice (N=3). After 24 h, mice were sacrificed and after saline perfusion, the main organs were extracted. *Ex vivo* fluorescence, as expected, revealed a large proportion of **7** in the liver and in spleen. Substantial accumulation of the probe was also observed in other organ of the RES system (kidney) and interestingly, a fraction also appears to target the brain (Supporting Information Figure S6). The results were confirmed by microscopy of histological organs sections stained with Prussian blue for iron detection. (Supporting Information Figure S6).

In Vivo Targeted Multimodal Imaging of Tumor in Mice with Selected BSA-NPs Contrast Agent (16). Due to the excellent colloidal properties and in vitro MRI/PET/OI contrast effects, we finally examined the multimodal imaging performance of one of the probes from the library for in vivo biomedical application. One advantage of the modular approach is the ease of further tailoring for biofunctionalization, for instance, the addition of a targeting ligand. Arginine-glycine-aspartic acid peptide (RGD) binds to the $\alpha_v\beta_3$ and $\alpha_v\beta_5$ integrins that are overexpressed in nascent endothelial cells during angiogenesis in various tumors, and yet not in inactive endothelial cells.[39] This property has been used many times for successful tumor and angiogenesis detection, with a wide range of probes from small chelators, polymeric nanoparticles, iron oxide nanoparticles, to quantum dots.[40] Thus, taking advantage of the presence of the maleimide-BSA module in the coating of **14**, RGD modified with a thiol functionality was covalently linked to the protein via a covalent thioether linkage with maleimide group.[41] $^{(DFO)(RGD)}$BSA-IONP (**16**) was labeled with ^{89}Zr and intravenously injected in tumor-bearing mice for PET/CT imaging and MRI. One hour after the injection high accumulation was found in the liver and spleen, as usual with imaging probes. It is also clear that a large fraction of the probe remained in systemic circulation. After 24 h, accumulation in tumor was observed with persistent and intense signal until 72 h, clearly delimiting the affected area (Figure 3a). For T_2-weighted MRI basal image and 24 h post injection are shown (Figure 3b). A loss of MRI signal intensity is clearly seen, especially delimiting the tumor.

The quantification in both types of images (PET and MRI) provides similar results. The tumor to muscle relative signal intensity in MRI clearly decays 24 h postinjection in a similar way in which the SUVmean (the decay corrected radioactive signal intensity from PET images) increases, in both cases as the $^{(89Zr)-(RGD)}$BSA-IONP (**16**) accumulates in the tumor (Figure 3c). The ex vivo radioactive signal of main organs was measured; Figure 3d shows the % injected dose as a function of the tissue weight for different organs. High signal in liver and spleen is observed, like we saw in the images, as well as in the tumor. Finally, bright field microscopy of different sections of the tumor harvested 72 h after i.v. injection revealed numerous Prussian blue stained areas (Supporting Information Figure S7). It allowed investigating the localization of **16** in the tumor. Distribution was heterogeneous (as already suggested by the PET and MRI) with a high uptake in the periphery, in accordance with the ensured RGD peptide targeting directed to the nascent endothelial cells.

CONCLUSIONS

Here we present a new approach for the modular multifunctionalization of different hydrophobic nanoparticles. This takes advantage of the parallel synthesis concept, rather than the traditional sequential process used in nanoparticles chemistry. In a single and rapid step, NPs are conjugated with native/modified BSA to prepare "ready to use" multifunctional nanoparticles. Using this modular albumin based platform, we have developed a wide library of contrast agents for cell labeling, drug delivery, and noninvasive imaging. Because of the ease and versatility of the route, a large range of BSA modules and ligands can be conjugated to the surface; therefore, it could convert to a routine methodology for preparation of a library of new molecular imaging agents. As an example, one of these candidates was selected and used for targeted PET/MRI multimodal in vivo imaging in a murine tumor model. Moreover, as a translational improvement in the field, the method presents notable advantages such as high reproducibility, facile scale-up production, and the use of biocompatible albumin coating. Finally, since albumin plays a role as a drug carrier in the clinical setting, our findings can be simply extended to incorporate new theranostic functions due to the versatility and high binding capacity of this protein. This modular proposal is very helpful, since it simplifies complex tailored functionalization and circumvents typical cumbersome problems associated with the reactions on the surface of the nanoparticles.

ASSOCIATED CONTENT

Supporting Information

Detailed experimental methods and supporting figures. This material is available free of charge via the Internet at http://pubs.acs.org.

AUTHOR INFORMATION

Corresponding Author

*E-mail: fherranz@cnic.es.

Author Contributions

All authors have given approval to the final version of the manuscript.

Notes

The authors declare no competing financial interest.

ACKNOWLEDGMENTS

This study is supported by a grant from FP7Marie Curie, Pulmonary imaging network (PINET), by a grant from Ministerio de Economía y Competitividad (MAT2013-47303-P) and by a grant from the Comunidad de Madrid (S2010/BMD-2326, Inmunothercan-CM). This work was partially funded by Instituto de Salud Carlos III (RETICS-RD12/0019/

0023 and RD12/0019/0005). We thank Dr. M. P. Morales (ICMM-CSIC) for TGA and VSM measurements. We thank E. Urones (Centro Nacional de Microscopía de la Universidad Complutense de Madrid) for the transmission electronic microscopy imaging.

■ ABBREVIATIONS

PET, positron emission tomography; MRI, magnetic resonance imaging; NP, inorganic nanoparticles; OA, oleic acid; OM, oleylamine; BSA, bovine serum albumin; IONP, iron oxide nanoparticles; UCNP, upconverting nanophosphors; AuNP, gold nanoparticles; DOTA, 1,4,7,10-tetraazacyclododecane-1,4,7,10-tetraacetic acid; DFO, deferoxamine; TEM, transmission electron microscopy

■ REFERENCES

(1) Lee, D.-E., Koo, H., Sun, I.-C., Ryu, J. H., Kim, K., and Kwon, I. C. (2012) Multifunctional nanoparticles for multimodal imaging and theragnosis. *Chem. Soc. Rev. 41*, 2656−72.

(2) De, M., Ghosh, P. S., and Rotello, V. M. (2008) Applications of nanoparticles in biology. *Adv. Mater. 20*, 4225−4241.

(3) Laurent, S., Forge, D., Port, M., Roch, A., Robic, C., Vander Elst, L., and Muller, R. N. (2008) Magnetic iron oxide nanoparticles: synthesis, stabilization, vectorization, physicochemical characterizations, and biological applications. *Chem. Rev. 108*, 2064−2110.

(4) Ghosh Chaudhuri, R., and Paria, S. (2012) Core/shell nanoparticles: classes, properties, synthesis mechanisms, characterization, and applications. *Chem. Rev. 112*, 2373−2433.

(5) Erathodiyil, N., and Ying, J. Y. (2011) Functionalization of inorganic nanoparticles for bioimaging applications. *Acc. Chem. Res. 44*, 925−935.

(6) Chen, Z., Chen, H., Hu, H., Yu, M., Li, F., Zhang, Q., Zhou, Z., Yi, T., and Huang, C. (2008) Versatile synthesis strategy for carboxylic acid−functionalized upconverting nanophosphors as biological labels. *J. Am. Chem. Soc. 130*, 3023−3029.

(7) Herranz, F., Morales, M. P., Roca, A. G., Desco, M., and Ruiz-Cabello, J. (2008) A new method for the rapid synthesis of water stable superparamagnetic nanoparticles. *Chem.—Eur. J. 14*, 9126−9130.

(8) Sperling, R. A., and Parak, W. J. (2010) Surface modification, functionalization and bioconjugation of colloidal inorganic nanoparticles. *Philos. Trans. R. Soc., A 368*, 1333−1383.

(9) Veiseh, O., Gunn, J. W., and Zhang, M. (2010) Design and fabrication of magnetic nanoparticles for targeted drug delivery and imaging. *Adv. Drug Delivery Rev. 62*, 284−304.

(10) Liong, M., Lu, J., Kovochich, M., Xia, T., Ruehm, S. G., Nel, A. E., Tamanoi, F., and Zink, J. I. (2008) Multifunctional inorganic nanoparticles for imaging, targeting, and drug delivery. *ACS Nano 2*, 889−896.

(11) Niemeyer, C. M. (2001) Nanoparticles, proteins, and nucleic acids: biotechnology meets materials science. *Angew. Chem., Int. Ed. 40*, 4128−4158.

(12) Groult, H., Ruiz-Cabello, J., Lechuga-Vieco, A. V., Mateo, J., Benito, M., Bilbao, I., Martínez-Alcázar, M. P., Lopez, J. A., Vázquez, J., and Herranz, F. F. (2014) Phosphatidylcholine-coated iron oxide nanomicelles for in vivo prolonged circulation time with an antibiofouling protein corona. *Chemistry,*.

(13) Longmire, M., Choyke, P. L., and Kobayashi, H. (2008) Clearance properties of nano-sized particles and molecules as imaging agents: considerations and caveats. *Nanomedicine 3*, 703−717.

(14) Thanh, N. T. K., and Green, L. A. W. (2010) Functionalisation of nanoparticles for biomedical applications. *Nano Today 5*, 213−230.

(15) Kratz, F. (2008) Albumin as a drug carrier: design of prodrugs, drug conjugates and nanoparticles. *J. Controlled Release 132*, 171−183.

(16) Peters, T. (1996) *All about albumin: biochemistry, genetics, and medical applications*, Academic Press, San Diego.

(17) Peng, Z. G., Hidajat, K., and Uddin, M. S. (2004) Adsorption of bovine serum albumin on nanosized magnetic particles. *J. Colloid Interface Sci. 271*, 277−283.

(18) Lynch, I., and Dawson, K. A. (2008) Protein-nanoparticle interactions. *Nano Today 3*, 40−47.

(19) Caravan, P., Cloutier, N. J., Greenfield, M. T., McDermid, S. A., Dunham, S. U., Bulte, J. W. M., Amedio, J. C., Looby, R. J., Supkowski, R. M., Horrocks, W. D., McMurry, T. J., and Lauffer, R. B. (2002) The interaction of MS-325 with human serum albumin and its effect on proton relaxation rates. *J. Am. Chem. Soc. 124*, 3152−3162.

(20) Schäffler, M., Sousa, F., Wenk, A., Sitia, L., Hirn, S., Schleh, C., Haberl, N., Violatto, M., Canovi, M., Andreozzi, P., Salmona, M., Bigini, P., Kreyling, W. G., and Krol, S. (2014) Blood protein coating of gold nanoparticles as potential tool for organ targeting. *Biomaterials 35*, 3455−3466.

(21) Gessner, A., Olbrich, C., Schröder, W., Kayser, O., and Müller, R. H. (2001) The role of plasma proteins in brain targeting: species dependent protein adsorption patterns on brain-specific lipid drug conjugate (LDC) nanoparticles. *Int. J. Pharm. 214*, 87−91.

(22) Mikhaylova, M., Kim, D. K., Berry, C. C., Zagorodni, A., Toprak, M., Curtis, A. S. G., and Muhammed, M. (2004) BSA immobilization on amine-functionalized superparamagnetic iron oxide nanoparticles. *Chem. Mater. 16*, 2344−2354.

(23) Xie, J., Chen, K., Huang, J., Lee, S., Wang, J., Gao, J., Li, X., and Chen, X. (2010) PET/NIRF/MRI triple functional iron oxide nanoparticles. *Biomaterials 31*, 3016−3022.

(24) Wilhelm, C., Billotey, C., Roger, J., Pons, J. N., Bacri, J.-C., and Gazeau, F. (2003) Intracellular uptake of anionic superparamagnetic nanoparticles as a function of their surface coating. *Biomaterials 24*, 1001−1011.

(25) Sanvicens, N., and Marco, M. P. (2008) Multifunctional nanoparticles − properties and prospects for their use in human medicine. *Trends Biotechnol. 26*, 425−433.

(26) Cheng, Z., Al Zaki, A., Hui, J. Z., Muzykantov, V. R., and Tsourkas, A. (2012) Multifunctional nanoparticles: cost versus benefit of adding targeting and imaging capabilities. *Science (80-) 338*, 903−910.

(27) Hao, R., Xing, R., Xu, Z., Hou, Y., Gao, S., and Sun, S. (2010) Synthesis, functionalization, and biomedical applications of multifunctional magnetic nanoparticles. *Adv. Mater. 22*, 2729−2742.

(28) Choi, J., Park, J. C., Nah, H., Woo, S., Oh, J., Kim, K. M., Cheon, G. J., Chang, Y., Yoo, J., and Cheon, J. (2008) A hybrid nanoparticle probe for dual-modality positron emission tomography and magnetic resonance imaging. *Angew. Chem., Int. Ed. 47*, 6259−6262.

(29) Yang, J., Lee, T.-I., Lee, J., Lim, E.-K., Hyung, W., Lee, C.-H., Song, Y. J., Suh, J.-S., Yoon, H.-G., Huh, Y.-M., and Haam, S. (2007) Synthesis of ultrasensitive magnetic resonance contrast agents for cancer imaging using PEG-fatty acid. *Chem. Mater. 19*, 3870−3876.

(30) Daniel, M.-C., and Astruc, D. (2004) Gold nanoparticles: assembly, supramolecular chemistry, quantum-size-related properties, and applications toward biology, catalysis, and nanotechnology. *Chem. Rev. 104*, 293−346.

(31) Liu, Y., and Welch, M. J. (2012) Nanoparticles labeled with positron emitting nuclides: advantages, methods, and applications. *Bioconjugate Chem. 23*, 671−682.

(32) Breeman, W. A. P., de Blois, E., Sze Chan, H., Konijnenberg, M., Kwekkeboom, D. J., and Krenning, E. P. (2011) ^{68}Ga-labeled DOTA-peptides and ^{68}Ga-labeled radiopharmaceuticals for positron emission tomography: current status of research, clinical applications, and future perspectives. *Semin. Nucl. Med. 41*, 314−321.

(33) Zhang, Y., Hong, H., and Cai, W. (2011) PET tracers based on Zirconium-89. *Curr. Radiopharm. 4*, 131−139.

(34) Sapsford, K. E., Algar, W. R., Berti, L., Gemmill, K. B., Casey, B. J., Oh, E., Stewart, M. H., and Medintz, I. L. (2013) Functionalizing nanoparticles with biological molecules: developing chemistries that facilitate nanotechnology. *Chem. Rev. 113*, 1904−2074.

(35) Zucker, R. M., Daniel, K. M., Massaro, E. J., Karafas, S. J., Degn, L. L., and Boyes, W. K. (2013) Detection of silver nanoparticles in

cells by flow cytometry using light scatter and far-red fluorescence. *Cytometry A*, DOI: doi: 10.1002/cyto.a.22342.
(36) Cho, E. C., Glaus, C., Chen, J., Welch, M. J., and Xia, Y. (2010) Inorganic nanoparticle-based contrast agents for molecular imaging. *Trends Mol. Med. 16*, 561−573.
(37) Fadeel, B., and Garcia-Bennett, A. E. (2010) Better safe than sorry: Understanding the toxicological properties of inorganic nanoparticles manufactured for biomedical applications. *Adv. Drug Delivery Rev. 62*, 362−374.
(38) Manshian, B. B., Moyano, D. F., Corthout, N., Munck, S., Himmelreich, U., Rotello, V. M., and Soenen, S. J. (2014) High-content imaging and gene expression analysis to study cell-nanomaterial interactions: The effect of surface hydrophobicity. *Biomaterials 35*, 9941−50.
(39) Gaertner, F. C., Kessler, H., Wester, H.-J., Schwaiger, M., and Beer, A. J. (2012) Radiolabelled RGD peptides for imaging and therapy. *Eur. J. Nucl. Med. Mol. Imaging 39*, 126−138.
(40) Liu, Z., and Peng, R. (2010) Inorganic nanomaterials for tumor angiogenesis imaging. *Eur. J. Nucl. Med. Mol. Imaging 37* (Suppl 1), S147−63.
(41) Kok, R. J., Schraa, A. J., Bos, E. J., Moorlag, H. E., Ásgeirsdóttir, S. A., Everts, M., Meijer, D. K. F., and Molema, G. (2002) Preparation and functional evaluation of RGD-modified proteins as $\alpha_v\beta_3$ integrin directed therapeutics. *Bioconjugate Chem. 13*, 128−135.